formed results permit an extension of theory to supercircular velocities. The ablation flight-test results at velocities up to 22,200 fps are in good agreement with the technique of predicting the cooling effectiveness of subliming ablators. However, further testing in the higher velocity regime is required to verify further the predictions.

Conclusions

The following conclusions are based on the results of several free-flight investigations wherein the thermal protection was provided by either a subliming ablator or by transpiration cooling: 1) The analogous behavior of subliming ablators to transpiration cooling permits direct comparison of these two types of heat protection; and 2) since the effectiveness of ablating materials is proportional to the mass injection rate and the vehicle velocity, extrapolation of the transpiration cooling effect based on relatively low-speed transpiration data, wherein high mass ejection rates were used, permits the prediction of material effectiveness to supercircular speeds.

References

[1] Winters, C. W. and Bracalente, E. M., "A sensor for obtaining ablation rates," NASA TN D-800 (1961).

[2] Walton, T. E., Jr., "Free-flight investigation of mass transfer cooling on a blunt cone to a Mach number of 10.6," NASA TN D-2197 (1964).

[3] Walton, T. E., Jr. and Rashis, B., "Measurement and empirical correlation of transpiration cooling parameters on a 25° cone in a turbulent boundary layer in both free flight and a hot-gas jet," NASA TN D-967 (1961).

[4] Howe, J. T. and Mersman, W. A., "Solutions of the laminar compressible boundary-layer equations with transpiration which are applicable to the stagnation regions of axisymmetric blunt bodies," NASA TN D-12 (1959).

[5] Rashis, B. and Hopko, R. N., "An analytical investigation of ablation," NASA TM X-300 (1960).

[6] Leadon, B. M. and Scott, C. J., "Measurement of recovery factors and heat transfer coefficients with transpiration cooling in a turbulent boundary layer at $M = 3.0$ using air and helium as coolants," Institute of Technology, Aeronautical Engineering Dept., Univ. of Minnesota Research Rept. 126(Contract AF 18(600)-1226) (February 1956).

[7] Witte, W. G. and Rashis, B., "An experimental investigation and correlation of the heat reduction to nonporous surfaces behind a porous leading edge through which coolant is ejected," NASA TM X-235 (1960).

[8] Brown, W. B. and Donoughe, P. L., "Tables of exact laminar-boundary-layer solutions when the wall is porous and fluid properties are variable," NACA TN 2479 (1951).

[9] Winters, C. W., Witte, W. G., Rashis, B., and Hopko, R. N., "Free-flight investigation of ablation of a blunt body to a Mach number 13.1," NASA TN D-1500 (1962).

SEPTEMBER-OCTOBER 1964 J. SPACECRAFT VOL. 1, NO. 5

Thermal Radiation from the Exhaust Plume of an Aluminized Composite Propellant Rocket

S. J. Morizumi* and H. J. Carpenter*
TRW Space Technology Laboratories, Redondo Beach, Calif.

A technique is developed for calculating rocket base heating and spacecraft heating environments due to particle radiation from a single nozzle exhaust plume. It has successfully predicted experimental results. The analysis treats radiation from a cloud of particles as that from an equivalent radiating surface. Thus, the problem is reduced to the determination of the proper values of the apparent surface emissivity and the effective temperature. In defining the apparent emissivity, an analogy with neutron scattering for a cylindrical cloud is adopted which shows the apparent emissivity to be dependent on particle emissivity and cloud optical thickness. Since the plume is nonuniform in particle size, concentration, and temperature, certain averaging techniques are used to define mean values of optical thickness and temperature. The particle flow-field information (particle concentrations, temperatures, and trajectories) necessary to determine these two quantities is provided by a two-phase flow-field computer program.

Nomenclature

a = $2\pi r_p/\lambda$
E = photon (radiant energy) flux, Btu/ft²-sec
F = shape factor from unshaded portion of particle plume to a surface element
I = radiant intensity, Btu/ft²-sec-sr-μ
k = cosine distribution exponent, Eq. (7)
L = total length of path across a particle plume, ft
L_0 = distance along view path from a surface element to particle plume boundary, ft
l = length through a particle plume, ft
m = number of plume segments
N = particle concentration, particles/ft³
$P_{i-1,k}$ = collision probability, Eq. (2)
P_n $\equiv P_{n,k}$
p_c = rocket chamber pressure, psia
p_e = ambient pressure, psia
Q = efficiency factor, Eq. (23)
$\dot{q}$ = radiant heat-transfer rate, Btu/ft²-sec
r = particle radius, ft or μ
T = absolute temperature, °R
x = distance along path from boundary of a particle cloud, ft

Presented as Preprint 64-61 at the AIAA Aerospace Sciences Meeting, New York, January 20–22, 1964; revision received March 31, 1964. The authors wish to express appreciation for the helpful discussions held with numerous members of the Space Technology Laboratories Technical Staff, and particularly for the computational assistance provided by Fern R. Bright and Mary L. Persons.

* Member of the Technical Staff. Member AIAA.

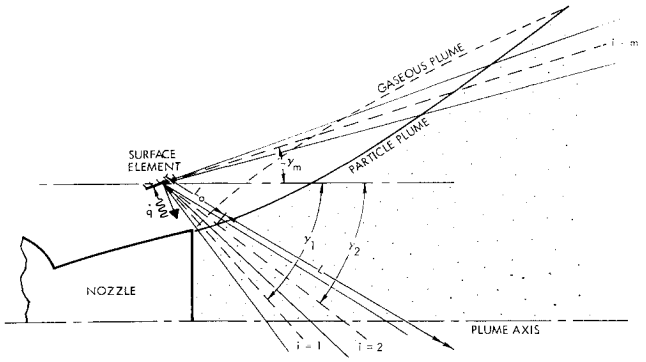

Fig. 1 Sketch of nozzle with gaseous and particle plumes, and surface element of base region.

α = absorptivity
β = neutron blackness (2)
γ = angle of plane of view with respect to plume axis, deg
ϵ = emissivity
η = temperature averaging factor
θ = directional angle, deg, Fig. 3
λ = wavelength, ft or μ
μ = $\cos\theta$
Π = infinite product symbol
ρ = reflectivity
σ = cross section, ft^2
σ_b = Stefan-Boltzmann constant, Btu/ft^2-sec-°R^4
τ = optical thickness
ϕ = dummy variable in integroexponential function; represents τ as used herein

Subscripts

a = apparent
i = dummy number
m = number of plume segments
M = maximum
n = one of five particle sizes
0 = initial or incident
p = particle
s = scattering
t = total or extinction
tr = transmitted
α = absorbed
λ = function of wavelength

Superscript

$\overline{(\ )}$ = average or effective

Introduction

WHEN aluminized composite propellant rockets are used to boost suborbital payloads or to inject spacecraft into final orbits, there is significant radiant heating from the exhaust to the rocket base and to the spacecraft. It is important to be able to predict these heating rates in order to design thermal insulation and shielding and to evaluate effects on solar cells, sensors, and other components. For altitudes above about 100,000 ft, it can be shown that heating of surfaces located forward of the rocket nozzle exit due to exhaust gas radiation is negligible compared to heating from aluminum oxide particle radiation, because of the relatively low temperature and emissivity of the expanded gases. The problem, then, is reduced to that of predicting the thermal radiation from the exhausted particle stream or "plume."

A technique sufficiently accurate for engineering design purposes has been developed and is the subject of this paper. The plume is treated as an equivalent surface radiator whose shape is that of the plume. The plume is divided into a number of segments by planes emanating from a surface element (Fig. 1). The increment of radiation incident to the surface element from each segment is determined by the familiar relation

$$\Delta\dot{q}_i = \Delta F_i \bar{\epsilon}_{a_i} \sigma_b \bar{T}_i^4 \tag{1}$$

A summation of radiation from all segments visible to the surface element yields the value of the total radiation.

The shape factor ΔF_i of each segment to the surface element is a function of the surface shape of the particle plume. Morizumi[1] has developed an analytical method for calculating shape factors to cones, hyperboloids, and segments thereof, which is used herein. The remaining two quantities, $\bar{\epsilon}_{a_i}$ and $\bar{T}_i$, are functions of not only the surface shape of the plume, but also the aluminum oxide particle concentrations and temperatures. Techniques used to arrive at all three quantities rely upon particle flow-field information (particle trajectories, concentrations, and temperatures) obtained by a two-phase-flow computer program.[2]

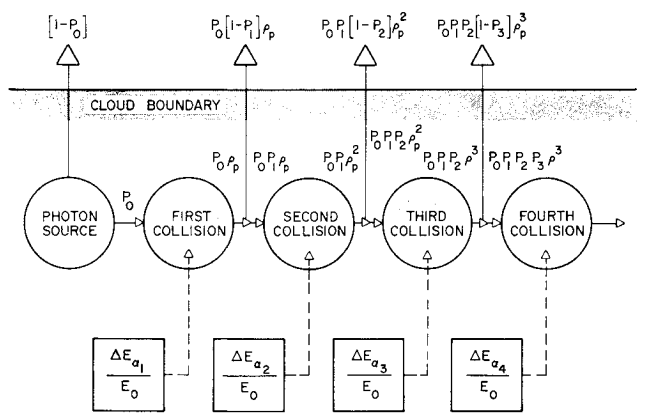

Fig. 2 Probability of photon absorption in a particle cloud.

Analytical Method

Apparent Emissivity

In determining the apparent emissivity of a particle cloud, an *analogy with neutron blackness* (probability of neutron absorption by a medium) is used. The neutron blackness utilizing the probability approach is expressed by Stewart[3,4] and Anthony[5] in their studies of the neutron scattering problem as

$$\beta = \frac{\sigma_\alpha}{\sigma_t} \sum_{j=1}^{\infty} \left(\frac{\sigma_s}{\sigma_t}\right)^{j-1} \prod_{i=1}^{j} P_{i-1,k}(\tau) \tag{2}$$

The collision probability $P_{i-1,k}$ is defined as the probability that a neutron that has experienced $(i-1)$ collisions with other particles in the medium will experience at least one more collision therein. The collision probability increases monotonically with optical thickness[3-5]; the latter is a measure of capture probability and is defined in the following section. A similar probability function can be used to define the radiant energy absorbed by a cloud of particles. In this case, the photons in the particle cloud are considered to replace the neutrons. As illustrated in Fig. 2, the radiant energy absorbed in the first collision of photons with particles is

$$\Delta E_{\alpha_1} = E_0(P_0 - P_0\rho_p) = E_0P_0(1 - \rho_p)$$

Likewise, the energy absorbed on each successive collision is

$$\Delta E_{\alpha_2} = E_0P_0P_1\rho_p(1 - \rho_p)$$
$$\vdots \qquad \vdots$$
$$\Delta E_{\alpha_n} = E_0P_0P_1 \ldots P_{n-1}\rho_p{}^{n-1}(1 - \rho_p)$$

The absorptivity or emissivity of the particle cloud is the ratio of the total absorbed energy to the total incident energy, which is defined as

$$\alpha_a = \epsilon_a = \left(\sum_{i=1}^{\infty} \frac{\Delta E_{\alpha i}}{E_0}\right) = (1 - \rho_p) \sum_{j=1}^{\infty} \rho_p{}^{j-1} \prod_{i=1}^{j} P_{i-1} \tag{3}$$

Equation (3) can be simplified by assuming that the particles are opaque, i.e., $\rho_p = (1 - \epsilon_p)$. Thus,

$$\epsilon_a = \epsilon_p \sum_{j=1}^{\infty} [1 - \epsilon_p]^{j-1} \prod_{i=1}^{j} P_{i-1} \tag{4}$$

A comparison of (4) with (2) shows an analogy between neutron blackness and apparent emissivity.

For both neutrons and photons, the change of intensity due to absorption and scattering is a function of particle total cross section and particle concentration. The total cross section is a measure of the energy taken away by an individual particle and consists of absorbing and scattering cross sections ($\sigma_t = \sigma_s + \sigma_a$). It is seen from (2) and (4) that the ratios of the neutron absorption and scattering cross sections to the total cross section are equivalent to the absorptivity and reflectivity, respectively, of a particle. The latter expression can be applied to any cloud geometry. The effects of the cloud shape, the total cross section, and the particle concentration are reflected in each of the probability functions $P_{i-1,k}$.

The determination of the first few *probability functions* is shown below for an infinite slab of particles. Consider a cylindrical beam of rays traversing a slab in the direction of θ with respect to a line perpendicular to the slab (Fig. 3). Take an element of this beam of length dx and cross section A at x distance from the boundary. The total number of particles in this element is $NAdx$ and the total cross section is $\sigma_t NAdx$. Then the fraction of energy removed in the element through absorption and scattering is

$$(N\sigma_t A dx/A) = N\sigma_t dx$$

Therefore,

$$I + (\partial I/\partial x)dx = I - (N\sigma_t dx)I$$

$$(\partial I/\partial x) = -(N\sigma_t)I \tag{5}$$

Integrating once,

$$I = I_0 e^{-N\sigma_t x} \tag{6}$$

where I_0 is intensity at $x = 0$.

If the usual cosine function distribution of the radiant energy intensity is assumed for entrant distribution, then the initial intensity I_0 may be defined in terms of a maximum intensity as a function of the cosine of directional angle θ:

$$I_0 = I_M(\cos\theta)^k = I_M\mu^k$$

Substituting this expression into Eq. (6), and combining the result with (5),

$$\partial I/\partial x = -N\sigma_t I_M \mu^k e^{-N\sigma_t x} \tag{7}$$

The energy loss per unit length along a path may be defined as

$$dE/dx = -2\pi(\partial I/\partial x)d\mu$$

Combining this equation with (7),

$$|dE| = -2\pi I_M N\sigma_t \mu^k e^{-N\sigma_t x}\, d\mu\, dx$$

The total energy loss for a plane wave traversing across the slab of thickness t is then determined by integrating the preceding differential equation over the slab thickness and the solid angle 2π sr as follows:

$$E_t = 2\pi I_M \int_0^t N\sigma_t \int_0^1 \mu^{k-1} \exp\left(\frac{-N\sigma_t z}{\mu}\right) d\mu dz \tag{8}$$

The total energy incident to the slab can be determined as

$$E_0 = 2\pi \int_0^1 I_0 d\mu = 2\pi I_M \int_0^1 \mu^k d\mu = \frac{2\pi I_M}{k+1} \tag{9}$$

The probability of photons colliding with particles on their first flight in the slab is

$$P_{0,k} = \frac{E_t}{E_0} = (k+1) \int_0^t N\sigma_t \int_0^1 \mu^{k-1} \exp\left(\frac{-N\sigma_t z}{\mu}\right) d\mu dz \tag{10}$$

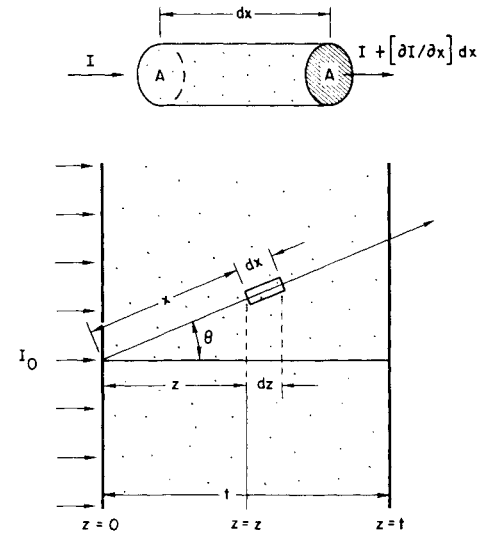

Fig. 3 Particle cloud geometry.

Thus, the probability function is dependent on the particle concentration, total cross section, and the cloud geometry.

In order to determine the second collision probability, the probability that photons reflected isotropically by a particle at a distance z escape through the surface $z = t$ without suffering further collision must be defined first. [This probability is denoted by $P(z)$.] If the intensity of the radiant energy reflected isotropically at $z = z$ is denoted by I_s, then the intensity of the energy transmitted from $z = z$ to the surface $z = t$ in the direction of θ may be expressed as

$$I_{tr} = I_s \exp[-N\sigma_t(t - z)/\mu]$$

The total energy transmitted from $z = z$ to $z = t$ is then determined as

$$E_{tr} = 2\pi \int_0^1 I_{tr} d\mu \tag{11}$$

and the total energy scattered at $z = z$ toward the surface $z = t$ is

$$E_s = 2\pi \int_0^1 I_s d\mu = 2\pi I_s \tag{12}$$

Thus,

$$P(z) = \frac{1}{2}\left(\frac{E_{tr}}{E_s}\right) = \frac{1}{2}\int_0^1 \exp\left[\frac{-N\sigma_t(t - z)}{\mu}\right] d\mu \tag{13}$$

where the factor of $\frac{1}{2}$ accounts for the half space. Similarly, the probability that photons reflected isotropically at $z = z$ escape through the surface $z = 0$ can be defined as

$$P'(z) = \frac{1}{2}\int_0^1 \exp\left(\frac{-N\sigma_t z}{\mu}\right) d\mu \tag{14}$$

Hence, the probability that once scattered photons escape through the surfaces $z = 0$ and $z = t$ is

$$P_{0,k}(1 - P_{1,k})\rho_p = \rho_p(k+1) \int_0^t N\sigma_t[P(z) + P'(z)] \int_0^1 \mu^{k-1} \exp\left(\frac{-N\sigma_t z}{\mu}\right) d\mu dz$$

The second collision probability, therefore, is

$$P_{1,k} = 1 - \left[\frac{(k+1)}{P_{0,k}}\right] \int_0^t N\sigma_t[P(z) + P'(z)] \times \int_0^1 \mu^{k-1} \exp\left(\frac{-N\sigma_t z}{\mu}\right) d\mu dz \tag{15}$$

By successive generations of the probability functions, the third collision probability can be similarly determined as

$$P_{2,k} = 1 - \left\{ (N\sigma_t/2)^2[(k+1)/(P_{o,k}\cdot P_{l,k})] \times \int_0^t [P(z) + P'(z)] \cdot \int_0^t \int_0^1 \mu^{k-1} \exp\left(\frac{-N\sigma_t z'}{\mu}\right) d\mu \times \int_0^1 \mu^{-1} \exp\left[\frac{-N\sigma_t(z-z')}{\mu}\right] d\mu dz' dz \right\} \quad (16)$$

The equations for the collision probability can be simplified by using the integroexponential functions, the values of which are readily available. The function is

$$\mathcal{E}_i(\phi) = \int_0^1 \mu^{i-2} e^{-\phi/\mu}\, d\mu$$

Thus, (10, 15, and 16) become

$$P_{0,k} = (k+1) \int_0^t N\sigma_t \mathcal{E}_{k+1}(N\sigma_t z) dz \quad (17)$$

$$P_{1,k} = 1 - \left[\frac{(k+1)}{2P_{0,k}}\right] \int_0^t N\sigma_t \mathcal{E}_{k+1}(N\sigma_t z) \cdot [\mathcal{E}_2(N\sigma_t z) + \mathcal{E}_2(N\sigma_t t - N\sigma_t z)] dz \quad (18)$$

$$P_{2,k} = 1 - \left(\frac{N\sigma_t}{2}\right)^2 \left[\frac{(k+1)}{(P_{0,k}\cdot P_{1,k})}\right] \int_0^t [\mathcal{E}_2(N\sigma_t z) + \mathcal{E}_2(N\sigma_t t - N\sigma_t z)] \int_0^t \mathcal{E}_{k+1}(N\sigma_t z') \mathcal{E}_1(N\sigma_t z - N\sigma_t z') dz' dz \quad (19)$$

It is apparent from these equations that the collision probability is a function of $(N\sigma_t t)$ and k. The parameter $(N\sigma_t t)$ is called "optical thickness." The parameter k is the exponent of the cosine function which represents the entrant distribution of radiant energy $k = 0$ for isotropic emission.

Variation of apparent emissivity with optical thickness and particle emissivity

Using the foregoing approach, Anthony and Stuart, respectively, developed the neutron blackness curves for the infinite slab and cylinder. The optical equivalent of these curves is presented in Fig. 4. The apparent emissivity for a constant particle emissivity is a monotonically increasing function of optical thickness τ. For large values of τ (optically thick cloud), the emissivity curves approach asymptotically a limiting value, regardless of the cloud geometry. For very small values of τ, however, the apparent emissivity differs for different geometry. For example a linearization of the apparent emissivity function results in the following approximations: $\epsilon_a = 1\epsilon_p\tau$ for a cylinder and $\epsilon_a = 2\epsilon_p\tau$ for a slab.

Although the configuration of a rocket exhaust particle plume resembles a cone, the emissivity for the cylindrical

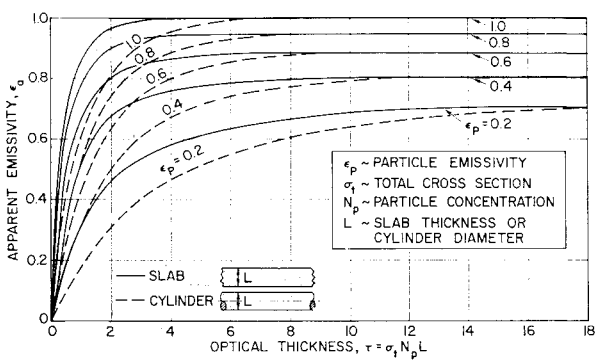

Fig. 4 Apparent emissivity for a cloud of particles in the form of a slab or a cylinder.

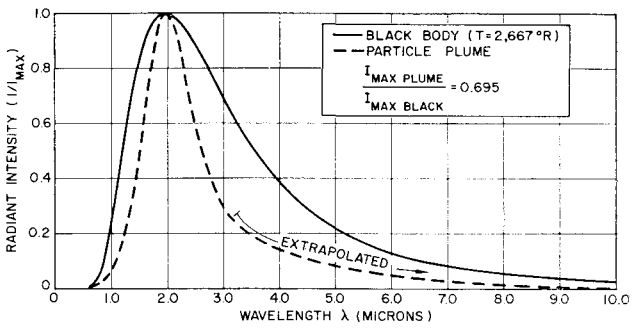

Fig. 5 Radiant intensity spectral distribution.

configuration is used here because the values of the probability functions for a cone are analytically intractable and because the axial symmetry of the cylinder approximates reasonably well the rocket plume geometry.

The *optical thickness* for a cloud of particles of uniform size and uniform concentration is defined as

$$\tau = N\sigma_t l \quad (20)$$

Inasmuch as the particle plume for a typical aluminized propellant rocket consists of varying size particles and, furthermore, the particle concentration is not uniform in the flow field, the optical thickness cannot be determined directly by use of the preceding expression. In computation of the particle plume flow field by the computer program,[2] five distinct particle sizes were used to simulate the actual flow field. Consequently, a superposition technique that sums up the thicknesses for all particle sizes has been adopted. The equation is

$$\tau = \sum_{n=1}^{5} \sigma_{ln} \int_0^{l_n} N_n(x) dx \quad (21)$$

where σ_t may be expressed in terms of the particle geometrical cross section as

$$\sigma_t = Q_t \pi r_p^2 \quad (22)$$

The coefficient Q_t is called the "extinction efficiency factor."[6, 7] It is a function of the particle size and shape, the refractive indices of the materials involved, and the radiation wavelength. The values of the total cross section for small carbon particles[8] and sapphire† spheres[9] have been determined by the Mie theory. According to the Mie theory, the extinction efficiency factor of a particle can be expressed as a function of $a = 2\pi r_p/\lambda$. As this value increases, the value of Q_t also increases for small values of a. If the imaginary part of the refractive index is small (small absorption coefficient), Q_t oscillates for intermediate values of a. However, for large values of a, the oscillation damps out and the value of Q_t becomes equal to 2.[6]

Based on Mie theory calculations for sapphire spheres,[9] Q_t oscillates about a mean value of 2 (or slightly greater) for $2 < a < 40$ with the amplitude relatively well damped above $a \approx 10$. The damping should be more rapid for aluminum oxide particles in a rocket exhaust because of their higher absorptive properties. From the continuous variation of both spectral radiant intensity (Fig. 5) and particle size in a rocket exhaust, it can be shown that a mean value of $Q_t = 2$ may be used. For $0 < a < 2$, Q_t varies between 0 and 2; however, since only a small part of the total radiation falls in this region for the particle plumes under consideration, its contribution to the mean value of Q_t is insignificant. Thus, σ_t in (21) is taken as twice the geometric cross section of the spherical particles.

Figure 4 shows that the *particle emissivity* can be equally important as τ in determining the apparent emissivity of a

† Aluminum oxide of single or few crystals.

particle cloud. A theoretical approach to the determination of particle emissivity is to apply the Mie theory to a sphere of appropriate size and observe the values of

$$\epsilon_{p_\lambda} = \sigma_{\alpha_\lambda}/\sigma_{t_\lambda} = Q_{\alpha_\lambda}/Q_{t_\lambda}$$

from which a total emissivity ϵ_p can be obtained. The values of Q_{α_λ} and Q_{t_λ} calculated for aluminum oxide (sapphire) spheres[9] result in a value of ϵ_p considerably less than 0.1. Higher values of particle emissivity determined grossly from measurements of rocket exhausts are in conflict with this result. It is suspected that the optical properties for sapphire are not representative of those for aluminum oxide particles in rocket exhausts. One argument that has been advanced is that the absorptive properties of the particles are higher than those of sapphire, due to a polycrystalline-porous structure of the former.[10] The high experimental values of particle emissivity seem to justify the assumption of opaqueness in (4).

For application to the present problem, a single value of $\epsilon_p = 0.25$ was chosen from the extrapolation of bulk aluminum oxide emissivity measurements. The single value is justified because of the small sensitivity of particle emissivity to temperature in the range of the temperature of the particles. Experimental data presented later tend to confirm the choice of $\epsilon_p = 0.25$.

The mechanics used to arrive at the particle emissivity from rocket plume measurements were as follows: Narrow angle radiometer measurements yielding $\dot{q}$ were made viewing across the exhaust plume near the nozzle exit. An average particle temperature along the line of view was determined as described below. The equation

$$\dot{q} = \bar{\epsilon}_a \sigma_b \bar{T}^4 \tag{23}$$

was then solved for $\bar{\epsilon}_a$. The value of τ along the line of view was determined as described previously. The effective particle emissivity was then determined by use of the cylinder curves of Fig. 4.

With the value of τ determined for any desired view through the axis of the particle plume, and with the value of ϵ_p determined as described previously, Fig. 4 can be used to obtain $\bar{\epsilon}_a$ for the plume segment encompassing that view. Each segment is treated as a cylindrical particle cloud whose axis is normal to the view line from the surface element through the center of that segment. The value of τ_i is computed based on the length of that view line l_n per Eq. (21). Then τ_i and ϵ_p are used, with the curves given in Fig. 4, for a cylindrical cloud to obtain a value of ϵ_{a_i} for the plume segment. The value of ϵ_{a_i} so derived is taken to be $\bar{\epsilon}_{a_i}$ for the segment surface, since the value of ϵ_a taken through the diameter of a cloud cylinder represents a mean value for that cylinder.[11]

Effective Plume Temperature

The particle temperature of an exhaust plume varies with particle size and particle location. Hence, an average temperature of particles along a given path is required to determine the heat rate from these particles. Since heat rates measured by narrow-angle radiometers are restricted to a small field of view of a cone about the instrument axis, an average temperature of particles along this axis will suffice to determine the heat rate to the instrument. However, for calorimeter (surface element) measurements, the field of view is hemispherical. Therefore, to determine a heat rate to a calorimeter, the temperature variations of the plume in lateral as well as longitudinal directions should be considered. The longitudinal variation is accounted for by segmenting the plume into a number of slices. However, the lateral variation is accounted for by applying an averaging correction factor to the average temperature of particles along a pencil view through the centerline.

Since a heat rate from a particle cloud to a given point is proportional to particle temperature to the fourth power, to particle concentration, particle cross section, and cloud thickness, and inversely proportional to the square of distance between the point of interest and an individual particle, the following averaging technique accounting for all these effects has been used to determine the effective temperature

$$\bar{T} = \left(\eta \frac{\int_{L_0}^{L_0+L} \sum_{n=1}^{5} N_n r^2_{p_n} T_{p_n}{}^4 \frac{dx}{x^2}}{\int_{L_0}^{L_0+L} \sum_{n=1}^{5} N_n r^2_{p_n} \frac{dx}{x^2}} \right)^{1/4} \tag{24}$$

The correction factor η is determined by taking the temperature variation in a lateral plane of view and averaging it over all view lines contained in that plane weighted by lateral variation of shape factor.

Total Radiation from Particle Plume

The total heat rate to a surface element is determined by integrating the heat rate from an infinitesimal slice of plume surface over the visible region of the plume. The equation is

$$\dot{q} = \int_{\gamma_0}^{\gamma_1} \epsilon_a[\tau(\gamma)]\sigma_b \bar{T}^4(\gamma) \left(\frac{dF}{d\gamma}\right) d\gamma \tag{25}$$

The integration may be performed numerically by segmenting the unshaded portion of the plume with a number of path planes extending from the surface element to the plume (Fig. 1.) For each of these segments, the mean values of τ_i, $\bar{\epsilon}_{a_i}$, and $\bar{T}_i$, can be determined. Shape factors ΔF_i from the surface element to these segments can also be determined.[1] Then, the total heat flux from the plume is determined as

$$\dot{q} = \sigma_b \sum_{i=1}^{m} \bar{\epsilon}_{a_i}(\tau_i) \bar{T}_i{}^4 \Delta F_i \tag{26}$$

Analytical Predictions and Experiments

Description of Experimental Tests

Experimental data were taken during the firing of two aluminized propellant rockets under simulated pressure altitude conditions. One rocket, the smaller (A), exhausted through a contoured nozzle of expansion ratio 19:1, which had an exit diameter of approximately 12 in. The second rocket (B) exhausted from a somewhat similar nozzle of expansion ratio 23.5:1 and exit diameter about 26 in. The chamber temperatures and the percentages of aluminum oxide in the exhausts were representative of those for typical aluminized propellants.

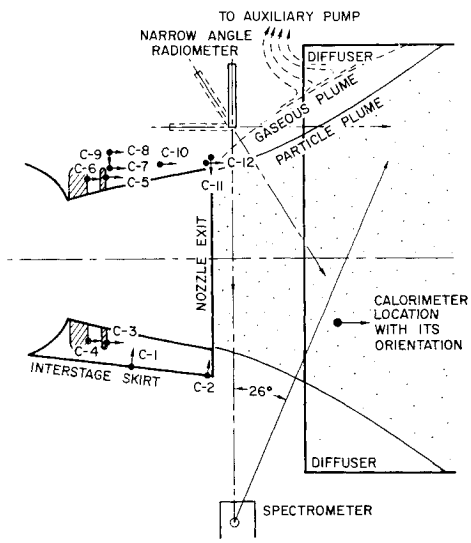

Fig. 6 Test arrangement and instrument locations: Rocket *B*.

The firings were made in a test cell arrangement that employed a diffuser and an auxiliary pumping system (Fig. 6.)

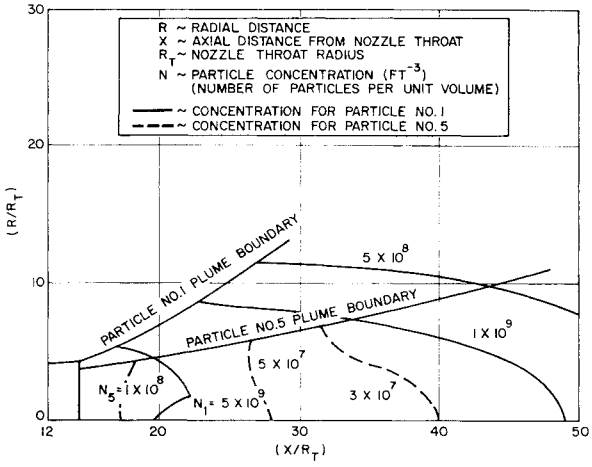

Fig. 7 Particle concentration distribution.

Average pressure altitudes of 110,000 and 130,000 ft were maintained during rocket *A* and rocket *B* firings, respectively. These altitudes were sufficiently high to permit expansion of the particle plume into as large a plume immediately downstream of the nozzle exits as would occur in a near vacuum. The recirculatory gas flow from the boundary of the exhaust gas plume was scavenged by the auxiliary pump, permitting only a small amount of convective heating in the area at and upstream of the nozzle exit.

A particle flow field was developed by the computer program[2] for the condition of each of the two rockets exhausting into a near vacuum ($p_e/p_e = 10^5$). In each case the particle size distribution was taken to be that given in Table 1. This distribution,[12] based on samples collected on glass slides during simulated firings of rockets containing similar propellant, results in a mean particle radius of 2.04 μ. Sample flow field information for the two extreme particle sizes are shown for rocket *B* in Figs. 7 and 8.

Instrumentation for measurement of thermal radiation was of three types: 1) narrow angle (5° solid angle) radiometers; 2) black surfaced asymptotic calorimeters; and 3) spectrometers that scanned the wavelength range 0.3 to 4.5 μ. Data used from the rocket *A* firing were taken by narrow-angle radiometers, which viewed across the particle plume 3 in. downstream of the nozzle exit and normal to the plume axial centerline. Data taken from the rocket *B* firing employed all three types of instruments. Figure 6 indicates the instrument locations for rocket *B*.

Experimental Results and Comparison with Analytical Predictions

The aluminum oxide *particle emissivity* was determined as described in the previous section from five radiometer measurements from the rocket *A* plume and from seven similar measurements from rocket *B*. Values are plotted in Fig. 9 along with emissivity measurements made on bulk alumina.[13]

Table 1 Particle size distribution

Particle number	Radius, μ	% total, Al_2O_3
1	0.79	20
2	1.28	20
3	1.76	20
4	2.44	20
5	3.95	20

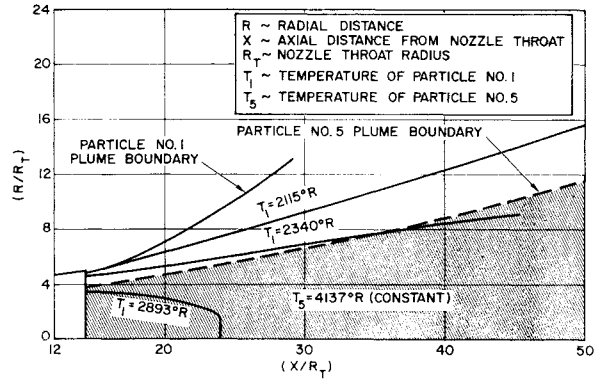

Fig. 8 Particle temperature distribution.

The reasonably good agreement between the two suggests that the particle emissivity approachs that of the bulk material rather than the low values of sapphire. This seems to corroborate the explanations given by others.[10, 14]

A value of particle emissivity was also determined by integrating the measured spectral intensities (Fig. 5) over wavelength and dividing by the integrated blackbody intensity. This value, $\epsilon_p = 0.3$, tends to confirm the radiometer measurements. The spectral data (Fig. 5) indicate that the plume radiation intensity decreases on either side of the peak wavelength at a rate faster than that of a black (or gray) body.

Using the analytical method developed in the previous section, the particle flow field for rocket *B*, and a particle emissivity of 0.25, predictions were made of *heat-transfer rates* to the calorimeters (surface elements) located as shown in Fig. 6. The effect of the presence of the diffuser was taken into account approximately in the following manner. The particle concentrations were assumed to remain constant downstream of the point at which the theoretical particle limiting trajectories intersect the diffuser wall, at values equal to those in the plane of that intersection. For purposes of determining τ and $\overline{T}$ for those segments that extend downstream along the length of the diffuser, the particle plume (constrained by the diffuser) was cut off at three nozzle exit diameters downstream of the nozzle exit, since downstream of this point, the values of $\overline{T}$ and τ (and therefore $\overline{\epsilon_a}$) would increase such a small amount that their effect on the contribution to $\dot{q}$ to the surface element from that segment is negligible.

Table 2 compares the predictions with experimental values measured during the firing of rocket *B*. The agreement is considered quite good for engineering predictions of heat rates. However, the rather large differences between predictions and experiment experienced on calorimeters 11 and 12 deserve further comment. It is believed that convective

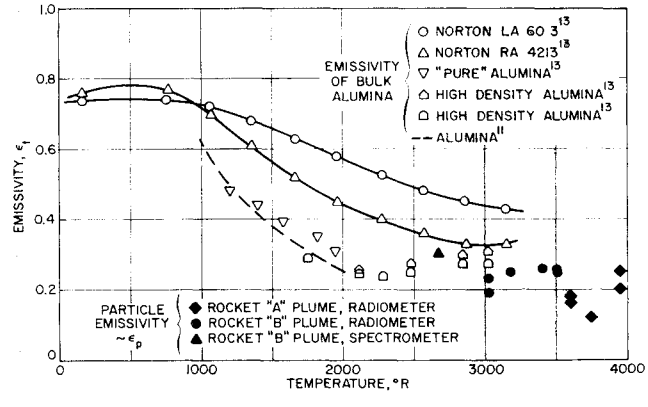

Fig. 9 Experimental values of aluminum oxide emissivity.

heating due to recirculation of hot gas inside the test cell, aluminum oxide slag protruding from the nozzle wall at its exit, and reflection from the supporting bracketry combined to increase the measured values. These effects have not been accounted for in the analytical predictions. Including these two measurements, the average difference between predictions and experimental values is 17% of the latter. If these two measurements are ignored, the difference is reduced to 14.2%.

Table 2 Comparison of predictions with experimental results[a]

Calorimeter	$\dot{q}_{\text{prediction}}$	$\dot{q}_{\text{test}}$	$(\dot{q}_{\text{prediction}}-\dot{q}_{\text{test}})/\dot{q}_{\text{test}}$
C-1	0.67	0.54	+0.241
C-2	7.00	5.78	+0.211
C-3	1.10	1.03	+0.068
C-4	1.05	0.83	+0.265
C-5	1.05	1.13	−0.071
C-6	1.12	1.03	+0.087
C-7	1.36	1.39	−0.022
C-8	1.76	2.12	−0.170
C-9	0.35	0.32	+0.094
C-10	2.50	3.10	−0.194
C-11	9.40	12.07	−0.221
C-12	5.00	8.35	−0.401

[a] Arithmetic mean of absolute values of deviation between test data and prediction: $\Delta\dot{q}/\dot{q} = 0.17$.

Application of Analytical Method

It is the opinion of the authors that the method developed here can be used to predict radiant heat rates incident to surfaces located in the region surrounding the plume of a wide range of particle-laden rocket exhausts. Examples are temperature-sensitive spacecraft surfaces and rocket aft closures and components located near the exhaust. Requirements are that the particle radiation level be so large compared to that of the gas that the latter is negligible and that the particle material and size distribution be known with sufficient accuracy to permit development of the flow field by means of a two-phase flow computer program. The particle emissivity must also be known.

Predictions should be suitably accurate for design purposes, except possibly for cases in which the surface elements are oriented such that they view only a small sector of the exhaust plume along its outer edge. An example of these surface elements is the outer surface of the nozzle wall (Fig. 1). It seems clear that, in this instance, the approximation of a plume segment by a cylindrical particle cloud is not valid. Fortunately the heat rates from the plume to surface elements so located are small and are usually not of major concern.

Conclusions

An approximate method has been developed which analytically predicts radiant heat rates incident to adjacent surfaces produced by a rocket exhaust containing a large percentage of its mass flow as aluminum oxide particles and operating in a rarefied atmosphere. Predictions can be made with accuracies suitable for engineering design.

The emissivity of aluminum oxide particles in a rocket exhaust appears to be between 0.1 and 0.3 at temperatures around 3500°R; this is not inconsistent with extrapolated data for bulk alumina.

An aluminum oxide particle plume at low ambient pressure radiates in a manner somewhat similar to a graybody. For wavelengths on either side of that at which the intensity peaks, the rate of intensity decay is considerably greater than that of a graybody.

References

[1] Morizumi, S. J., "Analytical method of determining shape factor from a surface element to a conical surface," Space Technology Labs., Internal Memo. 62-9721.4-78 (October 1962).

[2] Nickerson, G. R. and Kliegel, J. R., "The calculation of supersonic gas-particle flows in axi-symmetric nozzles by the method of characteristics," Space Technology Labs., Rept. 6120-8345-MUOOO (May 1962).

[3] Stewart, G. W., "Multiple scattering of neutrons," Nucl. Sci. Eng. **2**, 617–625 (1957).

[4] Stewart, G. W. and Woodruff, R. W., "Method of successive generations," Nucl. Sci. Eng. **3**, 339–373 (1958).

[5] Anthony, G. W., "The average escape probabilities for once and many-times scattered neutrons for a slab," General Electric Co., Hanford Atomic Products Operations Rept. HW-49188 (March 1957).

[6] Van de Hulst, H. C., *Light Scattering by Small Particles* (John Wiley and Sons, Inc., New York, 1957), Chap. VIII, pp. 107, 176–183.

[7] Stratton, J. A., *Electromagnetic Theory* (McGraw-Hill Book Co., Inc., New York, 1951), Chap. IX, p. 569.

[8] Stull, V. R. and Plass, G. N., "Emissivity of dispersed carbon particles," J. Opt. Soc. Am. **50**, 121–129 (Feb. 1960).

[9] Plass, G. N., "Mie scattering and absorption cross sections of aluminum-oxide and magnesium-oxide," Aeronutronic Div. of Philco Corp. Final Rept. SSD-TDR-62-127-V6 (May 1963).

[10] Lee, D. W. and Kingery, W. D., "Radiation energy transfer and thermal conductivity of ceramic oxides," J. Am. Ceram. Soc. **43**, 594–606 (1960).

[11] McAdams, W. H., *Heat Transmission* (McGraw-Hill Book Co., Inc., New York, 1954), 3rd ed., Chap. IV, pp. 88, 105.

[12] Kliegel, J. R., "Gas particle nozzle flows," *Ninth International Symposium on Combustion* (Academic Press, Inc., New York, 1963), pp. 811–826.

[13] Goldsmith, A., Waterman, T. W., and Hirschborn, H. J., *Handbook of Thermophysical Properties of Solid Materials* (Macmillan Co., New York, 1961), Vol. 3, Chap. VII, p. 43.

[14] Carlson, D. and Kuby, W., "An investigation of recombination and particle lag effects in rocket nozzles (*U*)," Aeronutronic Div. of Philco Corp. Fifth Quarterly Technical Summary Rept., Publication C-2265 (September 1963).